Evolution of dissolution processes at the interface of carbon steel corroding in a CO$_2$ environment studied by EIS

F. Farelas [a,b], M. Galicia [b,*], B. Brown [a], S. Nesic [a], H. Castaneda [c]

[a] Institute for Corrosion and Multiphase Technology, Ohio University, Athens, OH 45701, United States
[b] Instituto Mexicano del Petróleo, Eje Central Lázaro Cárdenas, San Bartolo Atepehuacan, México, DF 07730, Mexico
[c] Battelle Memorial Institute, Energy Systems, 505 King Avenue, Columbus, OH 43201, United States

ARTICLE INFO

ABSTRACT

The evolution of interfacial phenomena during CO$_2$ corrosion of C1018 carbon steel was characterized by EIS (Electrochemical Spectroscopy Impedance) and LPR (Linear Polarization Resistance). Turbulent conditions were simulated by a channel flow cell with deoxygenated 3 wt.% NaCl solution at 80 °C and pH 6 during 158 h. EIS helped in the characterization of the dynamic mechanism during the formation of the unprotective porous Fe$_3$C layer, and subsequent precipitation of the protective FeCO$_3$ layer inside the cementite. The experimental response of the active states at the interface was characterized by electrical passive elements with constant phase parameter analogs showing good agreement with the experimental results.

1. Introduction

Carbon dioxide corrosion of steel pipelines has been a serious problem in both the oil and gas industry for several years. Despite its low resistance compared with high corrosion resistance alloys (stainless steel, inconel, hastelloy, among others), carbon steel is widely used in the infrastructure for oil and gas industry, because of its cost effective characteristics. One of the inherent properties of this material is the formation of protective layers as a product of chemical and electrochemical reactions, when exposed to different environments [1,2]. Iron carbonate (FeCO$_3$) is one of such reaction products encountered, influencing the kinetics of the corrosion process by forming a porous physical barrier, between the electrolyte and the solid metallic surface. This barrier influences the transport of the corrosive species presented in the electrolyte [3]. The protectiveness of the porous layer depends on several environmental conditions, such as iron concentration, solution pH, temperature, partial pressure of CO$_2$, mechanical forces present in the flow and microstructure of the carbon steel [4–10].

Carbon and low-alloy steels chemical resistance in CO$_2$ environments depend on their microstructure and chemical composition. The formation of a coherent porous carbide (Fe$_3$C) layer with large surface area in steels with approximately 0.15% has been previously demonstrated [11–15]. Staicopolus [11] reported that the presence of cementite (Fe$_3$C) and ferrite (α-Fe) in steels can increment the corrosion rate; this effect is feasible due to the role of cementite as the cathodic site, while ferrite corrodes. One of the reasons for the latter is that Fe$_3$C is a metallic conductor with low hydrogen overvoltage [12]. Several investigations have focused on the effect of chemical composition of carbon steels on CO$_2$ corrosion leading their effort to the carbon content effect. Dugstad [13] found that ferritic–perlitic microstructures can be covered with a porous carbide phase, which remained unattacked on the surface when the steel was exposed in CO$_2$ environments. The presence of cementite was related to the relatively high carbon content on the steels studied. Al-Hassan et al. [14] studied the influence of microstructure on the corrosion rate of different carbon steels, finding that the corrosion rate increased with an increase in carbon content, due to the presence of a carbide phase. They also agreed that Fe$_3$C could be beneficial since it can act as a substrate for iron carbonate precipitation, anchoring the scale and protecting it against the flow shear stress. Gulbrandsen et al. [15] demonstrated that the efficiency of two imidazoline-based inhibitors was adversely affected by the presence of thick Fe$_3$C layers. Such layers increased in thickness with carbon content and they acted as a transport barrier for inhibitor compounds. In steels with relative low carbon content (<0.1%) the influence of the corrosion rate due to the presence of cementite is not considerable [16]. However, it is quite common to find carbon steels with carbon content >0.1% used for the elucidation of the corrosion mechanisms [17,18].

* Corresponding author. Tel.: +52 55 91 75 75 47; fax: +52 55 91 75 82 58.
E-mail address: galiciam@imp.mx (M. Galicia).

Previous studies have demonstrated that electrochemical impedance spectroscopy (EIS) can provide unique characterization of the electrochemical cell processes when there are different mechanisms and layers occurring at the interface [19–22]. Huang et al. [23,24] stressed the importance of EIS for getting quantitative information concerning the physical properties of inner barrier layers and outer porous layers on anodized aluminum 606.

In this work, the evolution of the interface of carbon steel exposed to CO_2 environment under turbulent conditions was characterized by means of electrochemical techniques for 158 h. The mechanisms occurred at the interface during dissolution and $FeCO_3$ film initiation-growth was related to the heterogeneous and chemical homogeneous reactions occurring on carbon steels with relatively high carbon content. LPR measurements were used to monitor the macroscopic changes and to estimate the corrosion rate with time and, qualitatively characterize the dissolution process, while the interface evolution of the different stages during the CO_2 corrosion of a C1018 carbon steel were characterized by EIS.

2. Experimental

2.1. System preparation and equipment

Experiments were conducted in a small volume (16 L capacity) flow loop called the "Thin Channel Flow Cell" or TCFC. The schematic layout of the system is shown in Fig. 1. The test section was built in the form of channel of rectangular shape, Fig. 2(a), the cell includes four locations for electrochemical probes and corrosion coupons to be flush mounted. It has a hydraulic diameter of 5.8 mm and was design to preserve the same flow conditions along the channel. Every test includes new volume of 30 L of 3 wt.% NaCl solution. Based on past studies that concentration has demonstrated to activate the dissolution process of carbon steels in CO_2 environments [25,26]. The 14 L left are used as a reservoir to provide make-up fluid for any losses that occur due to sampling for iron concentration or when the probes are inserted and removed from the test section. After the addition of solution and when the cell is filled, the pump is turned on. CO_2 was purged through the main tank and into the solution in the reservoir. Parallel with the purging process, the temperature was adjusted. The heat generated by the pump maintains the system up to 70–75 °C, then the temperature is adjusted and controlled by heaters in the tank and in the test section. When the desired temperature is achieved, and

the solution has been purged for 4 h, Chemet® ampoules are used for measuring the oxygen content of the solution sampled from the system. The oxygen concentration was measured and kept below 10 ppb. Continuous CO_2 injection is maintained in both the main tank and the reservoir during the test. The pH was continuously monitored in the flow stream between the pump and the test section. The pH of the test solution was adjusted by adding deoxygenated sodium bicarbonate solution ($NaHCO_3$). Flow rate was set at 0.5 m s^{-1} (1.1 Pa of shear stress) and kept constant during the test. This flow corresponds to fully developed turbulent flow with a Reynolds number of 8300. Then the electrochemical probe was flush mounted in the test section. All the experiments were duplicated to ensure results reproducibility. Experimental conditions are shown in Table 1.

2.2. Electrochemical probe preparation

The electrochemical probe is made by Metal Samples® and is designed as a concentric ring shape as displayed in Fig. 2(b). A non-conductive epoxy serves as an insulator between each electrode. The inner and middle rings are made from 1018 carbon steel and serve as the working and reference electrode, respectively. The outer ring is made with 316 stainless steel serving as the counter electrode. The working electrode (WE) has a 0.95 cm^2 exposed area. It has a carbon content of 0.16 wt.% that make it suitable for studying the formation of porous Fe_3C layers on steels exposed to CO_2 environments [13–18]. Chemical composition of the 1018 carbon steel is shown in Table 2. The electrochemical probe was polished by silicon carbide sand paper to a 600 grit surface finish and rinsed with isopropyl alcohol prior insertion to the TCFC.

2.3. Electrochemical measurements

Corrosion rates were measured electrochemically using the LPR technique. The carbon steel 1018 working electrode was polarized at ±5 mV. The scan rate was 0.125 mV s^{-1}. The LPR corrosion rate was calculated by using cathodic Tafel slope of 120 mV dec^{-1} and anodic Tafel slope of 40 mV dec^{-1}. These two magnitudes resulted in constant proportionality for "B" of 13 mV as previously reported [27,28]. The EIS measurements used a 5 mV amplitude (rms) with a frequency range of 10 kHz to 10 mHz with eight points per decade. All the electrochemical measurements were performed using a Gamry® PCI4/300 Potentiostat/Galvanostat/ZRA. The software ZView 3.1 (Scribner Associates) was used for analyzing the EIS results.

3. Results and discussion

3.1. LPR corrosion rate

The evolution of corrosion rate with time by the LPR technique for carbon steel 1018 exposed to a 3 wt.% NaCl solution saturated with CO_2 is displayed in Fig. 3. Error bars denote maximum and minimum values obtained in two tests. Initial corrosion rate (CR) was 3.0 ± 0.6 mm y^{-1}. After 0.5 h, 50 ppm of Fe^{2+} were added in the form of $FeCl_2 \cdot 4H_2O$. The addition of $FeCl_2 \cdot 4H_2O$ has been widely used with the aim of achieving higher concentrations of Fe^{2+} and increasing the supersaturation of iron carbonate [29–32]. The supersaturation value of $FeCO_3$ (S_{FeCO_3}) is defined as the degree of divergence from thermodynamic equilibrium, and it is represented by expression (1):

$$S_{FeCO_3} = [Fe^{2+}][CO_3^{2-}]/K_{sp} \tag{1}$$

where, $[Fe^{2+}]$ is the actual concentration of ferrous ions; $[CO_3^{2-}]$ is the equilibrium concentration of the carbonate ions; K_{sp} is the
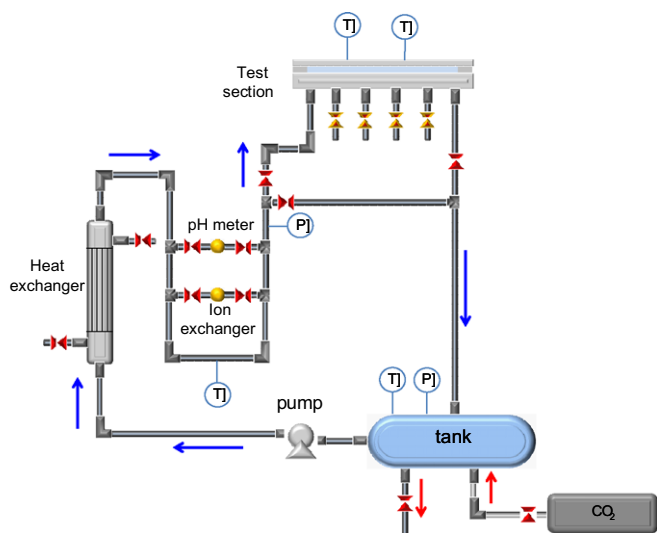

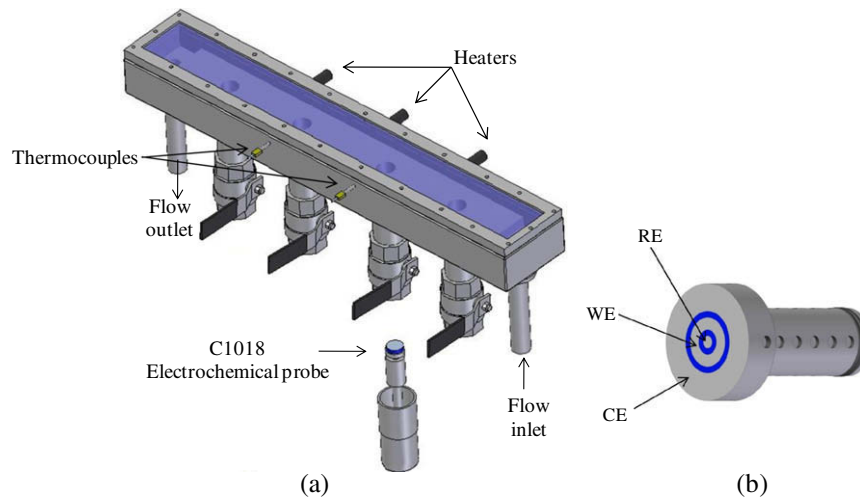**Fig. 1.** Schematic diagram of the thin channel flow cell.

Fig. 2. (a) Schematic representation of test section of the TCFC, (b) LPR probe head.

Table 1
Parameters and electrochemical techniques for the experimentation in the TCFC.

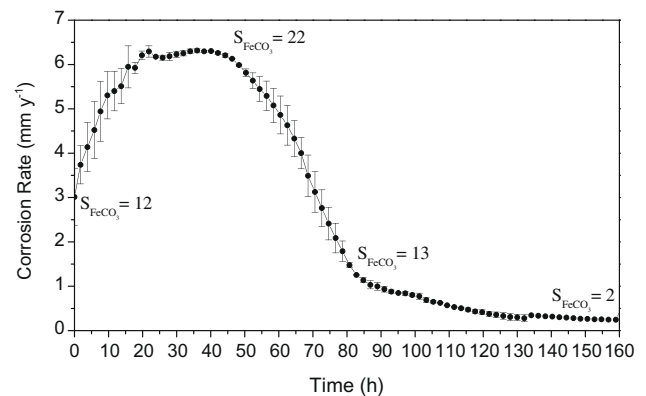| Parameters	Conditions
Total pressure	1 bar
pCO$_2$	0.54 bar
Temperature	80 °C
Flow rate	0.5 m s^{-1} (shear stress 1.1 Pa)
Solution	3 wt.% NaCl
pH	6 ± 0.10
Material	C1018
S(FeCO$_3$)$_{initial}$	12
Electrochemical measurements	
Linear polarization resistance (LPR)	±5 mV polarization, 0.125 mV s^{-1}
Electrochemical impedance spectroscopy (EIS)	5 mV amplitude (rms), 10 kHz–10 mHz

Fig. 3. Change of corrosion rate and supersaturation of FeCO$_3$, error bars denote maximum and minimum values in two tests (T = 80 °C, pCO$_2$ = 0.54 bar, pH = 6, 15 Pa shear stress, [NaCl] = 3 wt.%).

solubility product for FeCO$_3$ which is a function of temperature and ionic strength [29,30]. According to Eq. (1) the 50 ppm of Fe^{2+} ions added corresponds to a bulk initial FeCO$_3$ supersaturation of 12. In order to calculate the S_{FeCO_3} value at different times several iron concentration measurements were performed during the test. Variation of S_{FeCO_3} with time is shown in Fig. 3. CR increased to 6.2 ± 0.1 mm y^{-1} after 20 h of exposure suggesting a modification at the interfacial processes. Fig. 3 shows the relative constant magnitude for CR after 20 h of exposure with magnitude close to 6 mm y^{-1}. As a result of the corrosion process the concentration of Fe^{2+} ions in solution increased, resulting in S_{FeCO_3} value of 22. After 45 h the CR and S_{FeCO_3} value started to decrease. This latter marked a shift in the active state to slow kinetics for CR due to the formation of a protected layer at the interface electrode–electrolyte, two slopes represent the initiation and growth of a new corrosion product, the steeper slope displayed between 45 and 90 h can be attributed to the initiation of the formation of iron carbonate layer, the second slope is attributed to the growth of the layer and continuous decrease of CR until it stabilized at 0.2 ± 0.07 mm y^{-1} after 130 h that assumes the complete precipitation layer that slowed the CR.

3.2. EIS results

Corrosion rate measurements illustrate the evolution of the dissolution of the steel surface under controlled turbulent flow conditions in a CO$_2$ environment. AC impedance provided insight into the corrosion mechanisms occurring at the interface. The exposure time is divided into three different states, according to the interfacial processes and impedance signature. The states are: active adsorption, active-porous layer transition and mixed porous layer. The states are described in detailed.

3.2.1. Active-adsorption state
The active-adsorption state occurs when the steel sample is exposed to the CO$_2$ – electrolyte. Fig. 4(a) shows the Nyquist diagram of the C1018 steel for the first 20 h of exposure. Two time constants are identified; a capacitive semicircle in the high (HF)–med-

Table 2
Chemical composition of the 1018 carbon steels (wt.%).

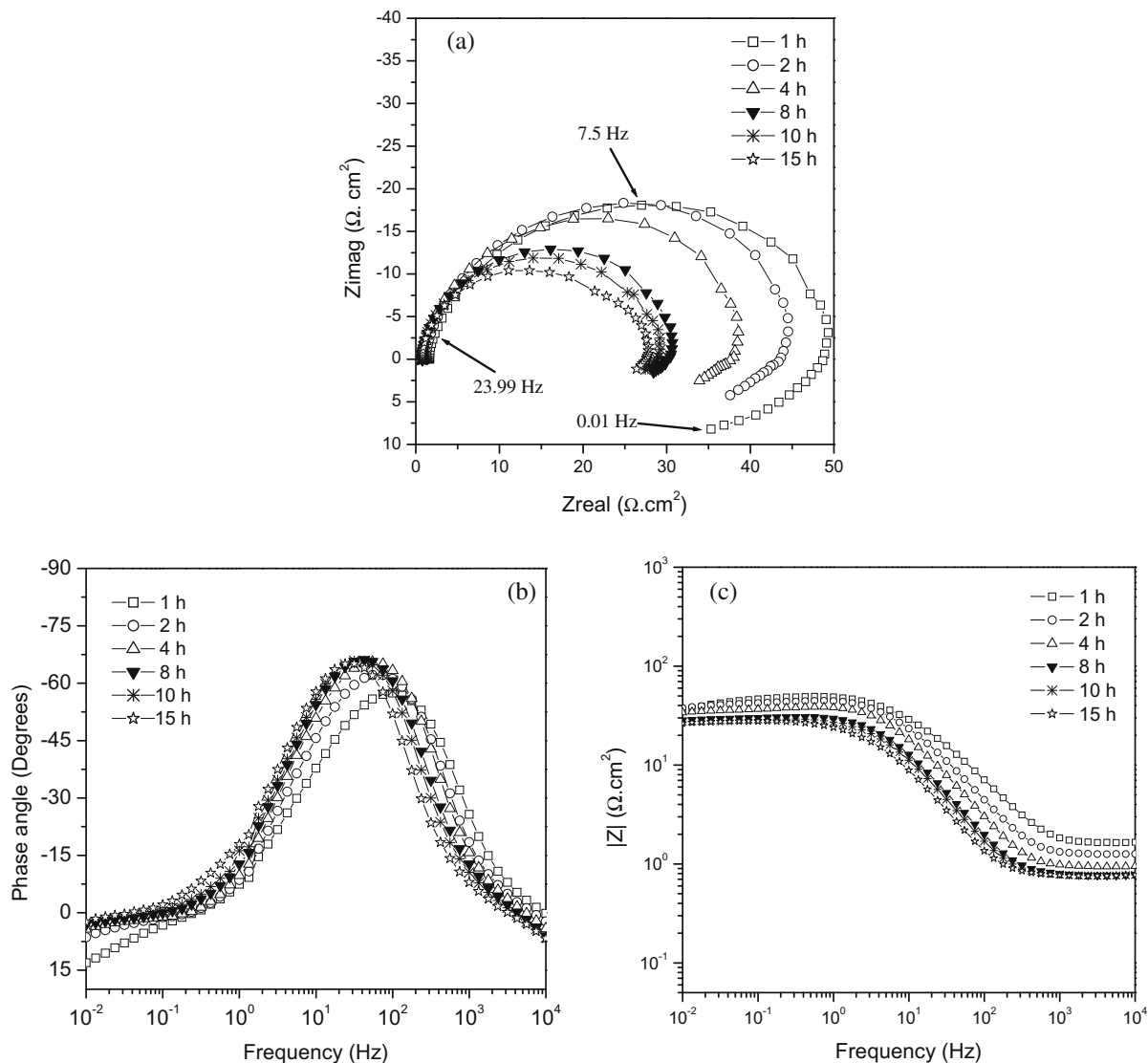| Al	As	C	Co	Cr	Cu	Mn	Mo	Nb	Ni	P
0.001	0.007	0.160	0.010	0.063	0.250	0.790	0.020	0.006	0.078	0.008
S	Sb	Si	Sn	Ti	V	Zr				
0.029	0.011	0.250	0.017	<0.001	0.001	0.004				

1018 Carbon steel (balance Fe)

Fig. 4. Impedance results obtained for a C1018 steel at different exposure times under turbulent conditions in a 3 wt.% NaCl solution saturated with CO_2: Nyquist (a) and Bode plots (b and c) representations.

ium (MF) frequencies range, and an inductive loop in the low frequency (LF) range. The capacitive semicircle characterizes the active state of the interface when steel is exposed to the CO_2 saturated solution. The amplitude of the loop decreases with respect to time, indicating that the charge transfer process assumed to be the cathodic reaction or hydrogen reduction is more favorable. This behavior has been related to the presence of Fe_3C which is part of the C1018 steel [33]. Fe_3C serves as an electronic conductor where the reduction of hydrogen ions takes place, following the intermediate reactions at the interface [34]. Cementite forms preferential cathodic sites with lower overpotential favoring hydrogen evolution. This leads to microgalvanic cells that are formed between Fe_3C and ferrite phase (α-Fe) resulting in selective dissolution of ferrite and the influence in the kinetics by galvanic effect [11,12,14]. The effect of cathodic regions of the cementite is considerable in carbon steels with carbon content higher than approximately 0.15% [35]. In this work the carbon steel used for electrochemical measurements has a carbon content of 0.16 wt.%. The increase in CR for the first 20 h observed in Fig. 3 is attributed to the galvanic effect of Fe_3C. A similar CR behavior was observed by Gulbrandsen et al. [15] on X65 and St52 carbon steels exposed to CO_2 environments. The increase in CR was related to the pres-

ence of cementite. They found a thicker cementite layer on St52 steel (C 0.13 wt.%) compared to the one found on X65 steel (C 0.064 wt.%).

The inductive loop observed in Fig. 4(a) at LF has been associated to the adsorption of an intermediate product on the metal surface according to the following reactions [36,37]:

$$Fe + H_2O \leftrightarrow FeOH_{ads} + H^+ + e^- \tag{2}$$

$$FeOH_{ads} \rightarrow FeOH_{sol}^+ + e^- \tag{3}$$

$$FeOH_{sol}^+ + H^+ \leftrightarrow Fe_{sol}^{2+} + H_2O \tag{4}$$

These reactions represent the active dissolution of the metal surface that follows the adsorption of an intermediate product $FeOH_{ads}$. The Nyquist plot, Fig. 4(a), shows the evolution of the impedance signature characteristic of inductive behavior. The signal in the fourth quadrant impedance signature disappears with time. Fig. 4(b and c) show the phase angle and Bode representation of the EIS spectra, respectively. Phase angle representation in Fig. 4(b) shows at HF–MF magnitudes characteristic of charge transfer process due to dissolution process. The phase angle evolution at LF shifts from negative to positive quadrant. Such transition is attributed to the control mechanisms at the interface; first the

adsorption process controls the interfacial process by means of the intermediate ions as represented in expression (3). The continuous formation of Fe_3C resulted in higher number of sites favorable for adsorption reaction and less favorable for the overall charge transfer process. The cathodic reaction represented in expression (5) controls the interfacial process due to the higher area of cementite and continuous dissolution of ferrite. As a consequence, reaction (4) is faster and no longer the control mechanism. The adverse effect of adsorption becomes significant as is manifested by the disappearance of the inductive loop [38].

$$H^+ + 2e^- \rightarrow H_2 \qquad (5)$$

The evolution of the interface for the first 15 h of exposure is characterized by the equivalent circuit (EC) represented in Fig. 5. This EC has been widely used for modeling the steel–CO_2 interface involving an adsorbed intermediate product [37,39], where R_s is the electrolyte resistance, Q_{dl} is a constant phase element (CPE) representing the double – charge layer capacitance, R_{ct} is the charge transfer resistance, R_L is the inductive resistance and L is the inductance. The CPE impedance (Z_{CPE}) is described by Eq. (6) as follows:

$$Z_{CPE} = 1/(Qj\omega)^n \qquad (6)$$

where Z_{CPE} is the impedance of CPE, Q is a proportional factor (CPE), "j" is $\sqrt{-1}$, ω is $2\pi f$, and n is a factor which takes values between 0 and 1. The slope of -0.93 in a plot of Log f (Hz) versus Log Z'' (Ω cm^2) at 8 h justifies the existence of a constant phase element [40,41]. As the imaginary part of the impedance is independent of the electrolyte resistance, the slope is constant in the frequency range.

The impedance parameters obtained following the fitting of the EIS experimental results by using the EC displayed in Fig. 5 are listed in Table 3. These parameters support the evolution of the active-adsorption surface resulted by the surface modifications for the cathodic reaction by assuming that the hydrogen evolved reaction (HER) is the cathodic reaction [42] and controls the interfacial process after 15 h of exposure. Q_{dl} increased from 183.49 to 1447.40 µF cm^{-2} s^{n-1} due to the physical–electrical properties of the corrosion products. Q_{dl} is directly proportional to the area available for the HER, the magnitude is also influenced by the increment in the cementite area, which is an electronic conductor [33,34]. R_{ct} decreased from 47.12 to 26.29 (Ohm cm^2) as a consequence of the continuous dissolution of the ferrite phase, and
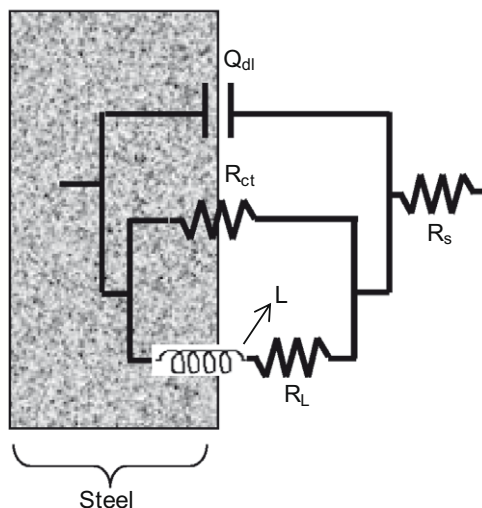

Fig. 5. Equivalent circuit used for modeling the EIS results from 1 to 15 h of exposure.

Table 3
Values of the elements of the equivalent circuit in Fig. 5 to fit the impedance spectra of Fig. 4.

Time (h)	Q_{dl} (µF cm^{-2} s^{n-1})	n_{Qdl}	R_{ct} (Ohm cm^2)	R_L (Ohm cm^2)
1	183.49	0.85	47.12	90.01
2	353.98	0.90	42.83	150.00
4	561.63	0.93	37.18	170.00
8	904.54	0.93	29.67	230.00
10	1087.50	0.93	28.02	235.00
15	1447.40	0.92	26.29	245.00

due to the increase of the cementite area which enhance the galvanic effect of Fe_3C [11,12,14]. R_L is directly proportional to the coverage of $FeOH_{ads}$ at the surface. The increase in CR due to the presence of Fe_3C causes the accumulation of $Fe(OH)_{ads}$ on the metal surface, and in the porous cementite with the later disappearance of the inductive loop [38].

3.2.2. Active-porous layer state

After 20 h of exposure CR stabilized at 6 mm y^{-1} and the S_{FeCO_3} value increased to 22, as displayed in Fig. 3. The increase in S_{FeCO_3} value is due to the corrosion process. Preferential dissolution of the ferrite phase over cementite causes the release of Fe^{2+} ions into the bulk solution, this increase in concentration of Fe^{2+} is directly proportional to the S_{FeCO_3} values according to Eq. (1) [29,30].

Fig. 6 shows the evolution of the EIS data after 20 h. The Nyquist representation in Fig. 6(a) shows two responses due to the influence of passive elements formed in the system, that are the result of the evolution of the dissolution process of the steel, and the porous cementite layer. The inductive loop is not present in the impedance spectra, and the appearance of a second loop with not defined amplitude is evident after 30 h of exposure. The MF–HF response is related to the characteristics of the porous cementite layer formed after the selective dissolution of ferrite, while the LF response is associated to the charge transfer process occurring at the steel–electrolyte interface. The two responses are represented in Fig. 6(b and c). Phase angle in Fig. 6(b) shows one maximum at MF, while at LF the increase of the phase angle magnitudes is attributed to the influence of a response at the interface due to HER. Two slopes are clearly seen in Bode representation diagrams after 30 h, indicating that more than one time constant resulted in the process [43].

The active-porous layer transition represented in the evolution of impedance signature in Fig. 6(a–c) is characterized by the equivalent circuit illustrated in Fig. 7 where: R_s is the electrolyte resistance, Q_c is the constant phase element describing the porous cementite layer, R_{po} is the pore resistance of the same layer, Q_{dl} is the constant phase element used to describe the double layer capacitance, and R_{ct} is the charge transfer resistance.

Table 4 displays the evolution of passive elements which are calculated after fitting the circuit analog proposed in Fig. 7. Q_c increase from 1868 to 3705 (µF cm^{-2} s^{n-1}). This magnitude is proportional to the increase of cementite surface and suggests that the maximum depth of the porous layer was reached at 50 h of exposure. Pots [16] has reported that typical cementite layer depths are close to 100 µm. Dugstad et al. [13,34] have shown evidence that ferritic–pearlitic normalized steel (0.15–0.18%C) were covered with a porous carbide film, which remained unattacked on the surface when the steel corrodes. Such porous films had approximately 60 µm depth. The pore resistance (R_{po}) kept constant indicating the formation of homogenous porous cementite layer. R_{ct} was relatively constant from 20 to 50 h; this latter trend confirms the LPR corrosion rate observed in Fig. 3 that was constant during the same time. The transition of the active surface to porous layer is influenced by the presence of the constant length
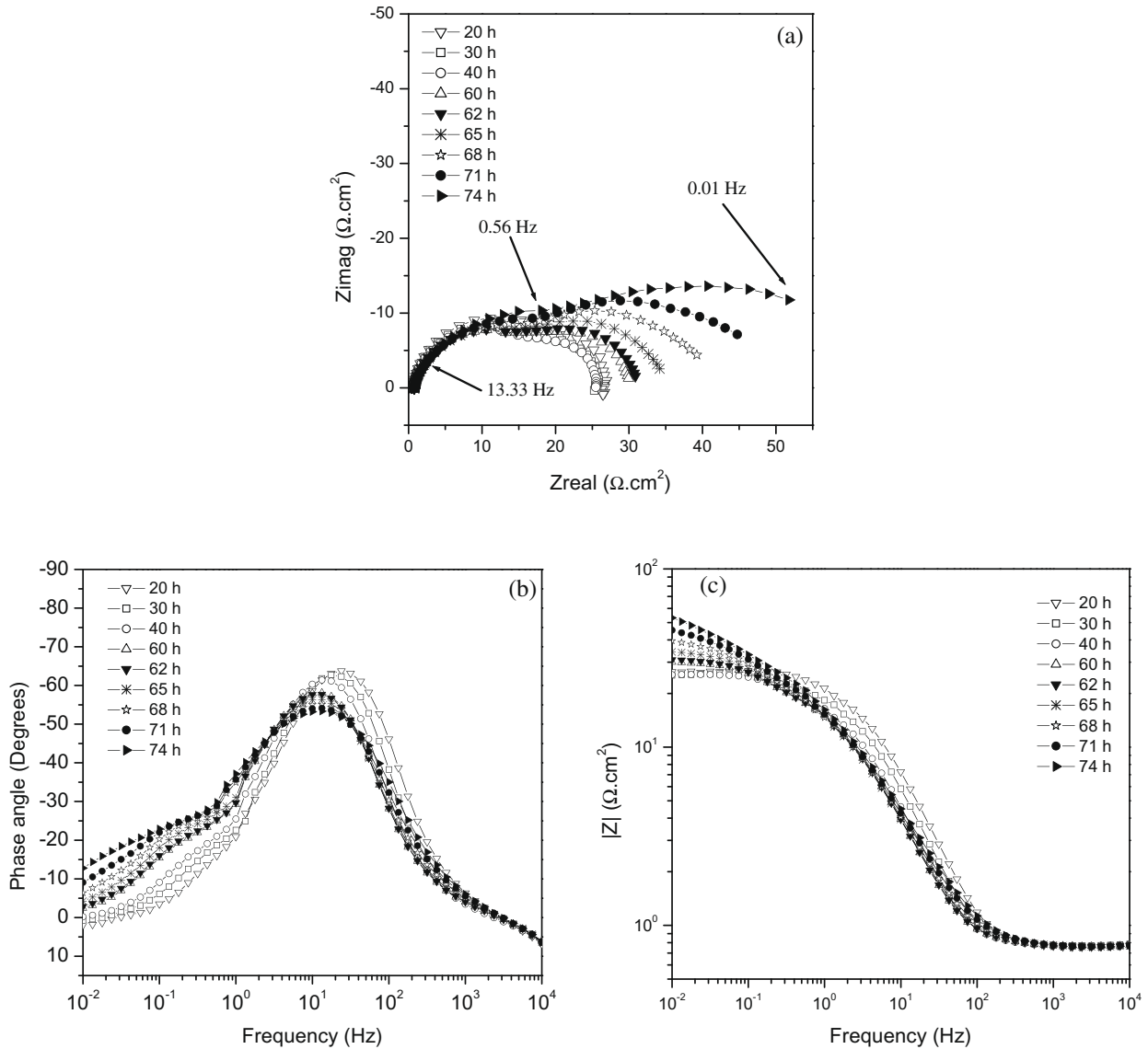
Fig. 6. Evolution of the EIS results obtained for a C1018 steel at different exposure times under turbulent conditions in a 3 wt.% NaCl solution saturated with CO_2: Nyquist (a) and Bode plots (b and c) representations.
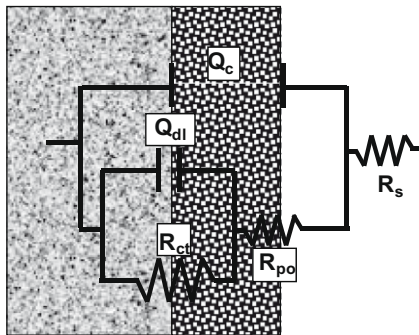

Fig. 7. Equivalent circuit used for modeling the EIS results from 20 to 74 h of exposure.

Table 4
Values of the elements of the equivalent circuit in Fig. 7 to fit the impedance spectra of Fig. 6.

Time (h)	Q_c ($\mu F\ cm^{-2}\ s^{n-1}$)	n_c	R_{po} (Ohm cm^2)	n_{dl}	R_{ct} (Ohm cm^2)
20	1868	0.97	17.94	0.97	7.80
30	2480	0.97	17.33	0.94	7.50
40	3160	0.93	17.84	0.95	7.01
50	3705	0.91	17.90	0.92	8.68
60	3620	0.90	17.45	0.85	12.18
62	3580	0.89	18.05	0.85	12.60
65	3420	0.86	19.16	0.84	15.01
68	3190	0.85	17.71	0.73	22.68
71	2880	0.84	18.17	0.65	31.20
74	2550	0.81	21.31	0.61	42.61

of the pores of the Fe_3C layer. After 60 h the passive elements and parameters shifts trends, the initiation of the $FeCO_3$ precipitation is

assumed at this time. The n_{dl} parameter started to decrease from capacitive behavior to pseudo-capacitance characteristic magnitudes [19] when scaling or precipitates are formed at the interface. The formation of new product is considered between 50 and 60 h due to the highest S_{FeCO_3} as displayed in Fig. 3. The R_{ct} corroborates the charge transfer reaction increment, due to different interface

formed at the base of the pore, the formation of $FeCO_3$ [13,44]. Table 4 shows the properties of the Fe_3C layer after 60 h, the Q_c and R_{po} are influenced by the initiation of a mixed layer formed by Fe_3C and the $FeCO_3$.

3.2.3. Mixed porous layer

After 80 h of exposure the interfacial mechanism evolves and modifies the impedance properties, the corrosion rate decreases, becoming virtually constant as illustrated in Fig. 3. Fig. 8(a) shows two loops with different amplitudes. The HF shows a small semicircle and MF–LF displays the second loop with higher amplitude. The Bode format displayed in Fig. 8(b) and phase angle in Fig. 8(c) corroborate the presence of two responses. The former illustrates two maxim points; the maximum at MF remains relatively constant while the maximum at LF increases with time. Fig. 8(c) shows two slopes characteristic of different time constants presented in the system. The HF loop in Fig. 8(a) and HF–MF in the other representations is related to the mixture of the layers, due to the precipitation of $FeCO_3$ inside the porous Fe_3C layer. The carbide phase depth and the physical characteristics of the mixture of two layers remained relative constant as represented in Fig. 8(b) at MF–HF, where no changes in the phase angle are observed. The increase in the capacitive loop at LF is illustrated in Fig. 8(a), the increase

in phase angle and the modulus of the impedance seen in Fig. 8(b) and (c), respectively at LF are attributed to the continuous precipitation of $FeCO_3$ inside the cementite layer, which increases the charge transfer resistance, due to the cathodic reaction (HER) by blocking charge transfer sites. The iron carbide porous layer influence the concentration gradient within the pores of the solution in contact with the metal, that can lead to local increase of pH and ion iron concentration gradient, allowing the formation of $FeCO_3$ between the cementite pores as demonstrated by previous works [13,35,44,45].

The experimental EIS results in the mixed porous layer were modeled by the EC displayed in Fig. 9. The EC proposed represents the evolution of the precipitation of $FeCO_3$ inside the carbide phase and its effect on the metal dissolution. R_s is the electrolyte resistance, Q_{ic} is the constant phase element describing the mixture of $Fe_3C + FeCO_3$, R_{po} is the pore resistance of the mixture layer, Q_{dl} is the constant phase element used to describe the double layer, and R_{ct} is the charge transfer resistance that describes the dissolution of the metal. The data obtained with the proposed EC showed good agreement with the experimental results as seen in Fig. 10.

Table 5 lists the evolution of the passive elements obtained with the EC shown in Fig. 9. Q_{ic} and R_{po} remains with small modification during the growth of the $FeCO_3$ layer precipitating and covering
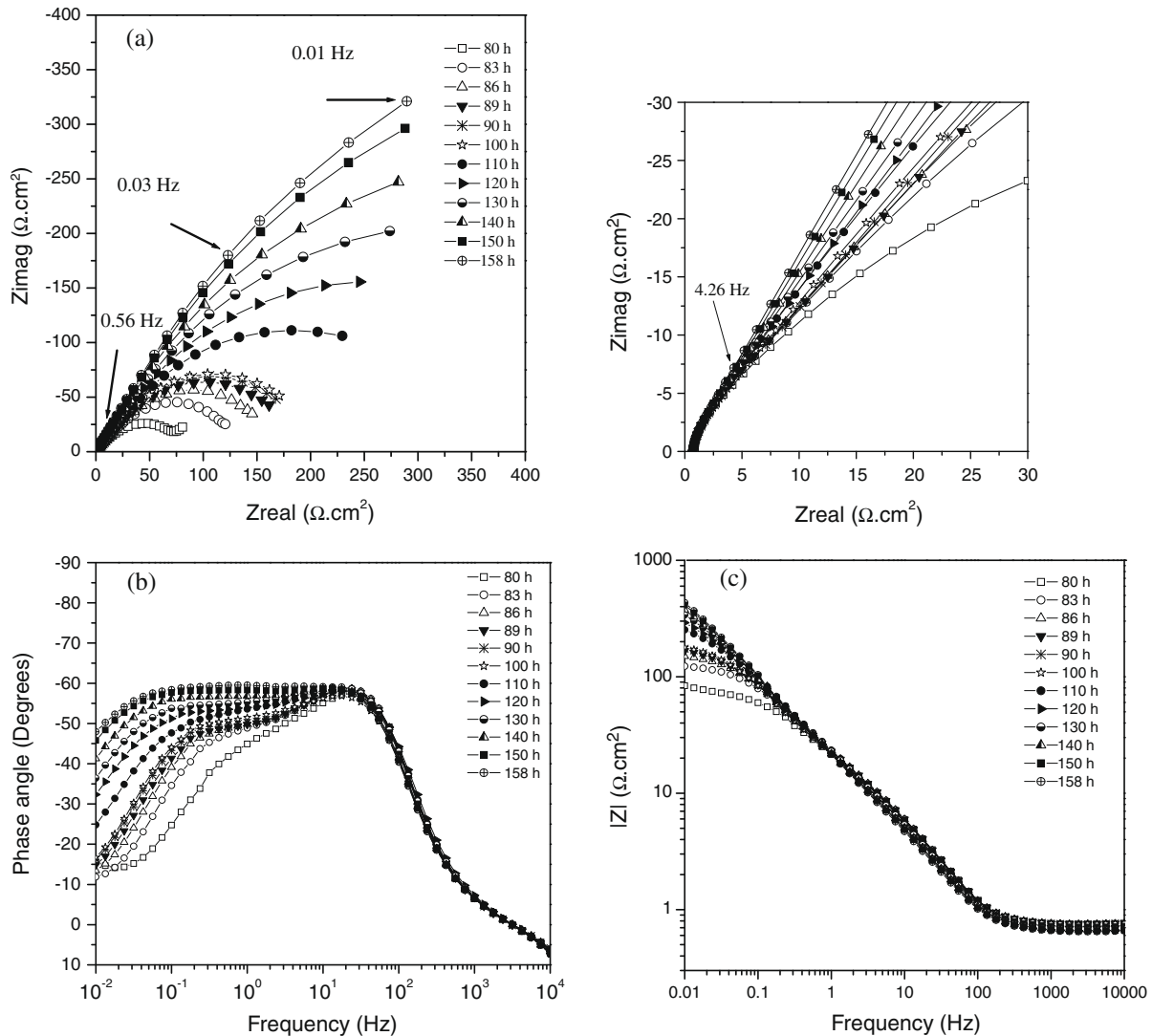

Fig. 8. Impedance results obtained for C1018 steel at different exposure times under turbulent conditions in a 3 wt.% NaCl solution saturated with CO_2: Nyquist (a) and Bode plots (b and c) representations.
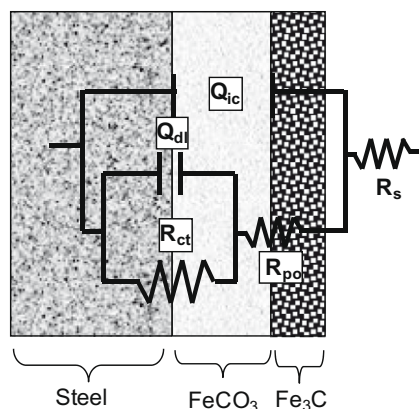
Fig. 9. Equivalent circuit used for modeling the EIS results from 80 to 158 h of exposure.

the Fe_3C pores. It has been reported that the adherence of $FeCO_3$ is related to the presence of cementite. The carbide phase strengthens the film and anchors it to the steel substrate [45,46]. Dugstad [13,44] has reported SEM pictures of carbon steels exposed to CO_2 environments showing cementite layers with the presence of $FeCO_3$. He found that ferritic–pearlitic normalized steel were covered with a porous carbide film filled with iron carbonate that formed close to the metal at 80 °C. This type of films ($FeCO_3$–

Fe_3C) is the most common mixture found on carbon and low-alloy steel surfaces in CO_2-containing environments [47]. $FeCO_3$ influences the active sites for cathodic reactions as represented in the phase angle at LF in Fig. 8(b) by the increase in magnitudes close to 45°. Q_{dl} decreases with time, due to the denser layer formed at the base of the pore blocking the active sites of the steel. The charge transfer resistance R_{ct} increases as the $FeCO_3$ grows at the pore. The R_{ct} and Q_{dl} magnitudes corroborate the CR evolution with time between 80 and 158 h of exposure.

4. Conclusions

The evolution of the dissolution process of steel exposed to CO_2 environment includes three different stages due to the mechanisms and processes existing at the interface.

Corrosion rate of bare mild steel electrodes increased initially, due to the selective dissolution of the ferrite phase leaving the iron carbide (cementite) structure intact. The latter caused a galvanic coupling effect, increasing the surface availability for the cathodic reaction and the formation of thick porous layer. Eventually a protective layer of iron carbonate formed within the pores of the iron carbide layer, significantly reducing the corrosion rate.

The information obtained by electrochemical impedance helped in the characterization of the dynamic mechanism during the formation of the unprotective porous iron carbide layer, and subsequent precipitation of the protective iron carbonate layer inside the cementite.
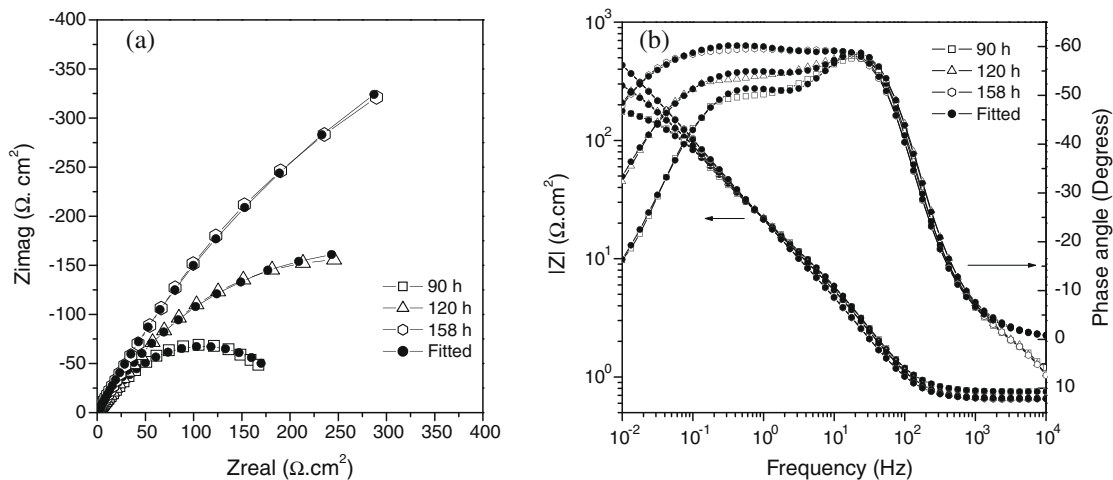

Fig. 10. Nyquist diagrams (a) and Bode plots (b and c) of C1018 at different exposure times under turbulent conditions in a 3 wt.% NaCl solution saturates with CO_2, a comparison of experimental data with the fitted results.

Table 5
Values of the elements of the equivalent circuit in Fig. 9 to fit the impedance spectra of Fig. 8.

Time (h)	Q_{ic} ($\mu F\,cm^{-2}\,s^{n-1}$)	R_{po} (Ohm cm^2)	Q_{dl} ($\mu F\,cm^{-2}\,s^{n-1}$)	n_{dl}	R_{ct} (Ohm cm^2)
80	1862	6.76	1101	0.65	81.89
83	1940	10.85	1670	0.70	128.40
86	1950	11.57	1660	0.70	164.00
89	1940	12.03	1690	0.69	188.60
90	1980	11.58	1780	0.69	203.10
100	2080	11.40	1630	0.69	210.80
110	1990	8.73	900	0.64	384.10
120	2020	7.77	960	0.63	572.90
130	2110	8.75	900	0.64	778.10
140	2250	7.99	970	0.65	1037.00
150	2310	7.33	940	0.65	1476.00
158	2390	6.77	870	0.65	1786.00

The corrosion product mixture layers are influenced by the pores formation with time, further studies focusing on pores properties should be considered.

Acknowledgments

References

[1] A. Pfenning, R. Bäßler, Effect of CO_2 on the stability of steels with 1% and 13% Cr in Saline Water, Corros. Sci. 1 (2009) 1, doi:10.1016/j.corsci.2009.01.025.

[2] K. Gao, F. Yu, X. Pang, G. Zhang, L. Qiao, W. Chu, M. Lu, Mechanical properties of CO_2 corrosion product scales and their relationship to corrosion rates, Corros. Sci. 50 (2008) 2796.

[3] M. Nordsveen, S. Nešić, R. Nyborg, A. Stangelend, A mechanistic model for carbon dioxide corrosion of mild steel in the presence of protective iron carbonate films – Part 1: theory and verification, Corrosion 59 (2003) 5.

[4] K. Videm, A. Dugstad, Corrosion of carbon steel in an aqueous carbon dioxide environment, Part 1: solution effects, MP 28 (3) (1989) 63.

[5] K. Videm, A. Dugstad, Corrosion of carbon steel in an aqueous carbon dioxide environment, Part 2: film formation, MP 28 (4) (1989) 46.

[6] M.L. Johnson, M.B. Tomson, Ferrous Carbonate Precipitation Kinetics and Its Impact CO_2 Corrosion, CORROSION/91, Paper No. 268, NACE, Houston, TX, 1991.

[7] V. Ruzic, M. Veidt, S. Nesic, Protective iron carbonate films – Part 2: chemical removal by dissolution in single-phase aqueous flow, Corrosion 62 (7) (2006) 598.

[8] S. Nesic, L. Lunde, Carbon dioxide corrosion of carbon steel in two-phase flow, Corrosion 50 (9) (1994) 717.

[9] V. Ruzic, M. Veidt, S. Nesic, Protective iron carbonate films – Part 1: mechanical removal in single-phase aqueous flow, Corrosion 62 (5) (2006) 419.

[10] Srdjan Nesic, Key issues related to modeling of internal corrosion of oil and gas pipelines – A review, Corros. Sci. 49 (2007) 4308–4338.

[11] N. Staicopolus, The role of cementite in the acidic corrosion of steel, J. Electrochem. Soc. 110 (1963).

[12] K. Videm, J. Kvarekvaal, T. Pérez, G. Fitzsimons, Surface Effects on the Electrochemistry of Iron and Carbon Steels Electrodes in Aqueous CO_2 Solutions, CORROSION/96, Paper No. 1, NACE, Houston, TX, 1996.

[13] A. Dugstad, Mechanism of Protective Film Formation During CO_2 Corrosion of Carbon Steel, CORROSION/98, Paper No. 31, NACE, Houston, TX, 1998.

[14] S. Al-Hassan, B. Mishra, D.L. Olson, M.M. Salama, Effect of microstructure on corrosion of steels in aqueous solutions containing carbon dioxide, Corrosion 54 (6) (1998) 480.

[15] E. Gulbrandsen, S. Nesic, A. Stangeland, T. Burchardt, Effect of Precorrosion on the Performance of Inhibitors for CO_2 Corrosion of Carbon Steel, CORROSION/98, Paper No. 13, NACE, Houston, TX, 1998.

[16] B.F.M. Pots, Mechanistic Models for the Prediction of CO_2 Corrosion Rates Under Multi-Phase Flow Conditions, CORROSION/95, Paper No. 137, NACE, Houston, TX, 1995.

[17] A. Fragiel, R. Schouwenaarf, R. Guardian, R. Perez, Microstructural characteristics of different commercially available API 5L X65 steels, J. New Mater. Electrochem. Syst. 8 (2005) 115–119.

[18] D. Clover, B. Kinsella, B. Pejcic, R. de Marco, The influence of microstructure on the corrosion rate of various carbon steels, J. Appl. Electrochem. 35 (2005) 139–149.

[19] G. Li, H. Ma, Y. Jiao, S. Chen, An impedance investigation of corrosion protection of copper by self-assembled monolayers of alkanethiols in aqueous solution, J. Serb. Chem. Soc. 69 (10) (2004) 791–805.

[20] T.K. Rout, Electrochemical impedance spectroscopy study on multi-layered coated steel sheets, Corros. Sci. 49 (2007) 794.

[21] Y. Chen, H.J. Chen, W.P. Jepson, Effect of Multiphase Flow on Corrosion Inhibitor, CORROSION/99, Paper No. 12, NACE, Houston, TX, 1999.

[22] T. Hong, H. Shi, H. Wang, M. Gopal, W. P. Jepson, EIS Study of Corrosion Product Film in Pipelines, CORROSION/2000, Paper No. 44, NACE, Houston, TX, 2000.

[23] Y. Huang, H. Shih, H. Huang, J. Daugherty, S. Wu, Evaluation of the resistance of anodized aluminum 6061 using electrochemical impedance spectroscopy (EIS), Corros. Sci. 50 (2008) 3569–3575.

[24] Y. Huang, H. Shih, J. Daugherty, F. Mansfeld, Evaluation o the properties of anodized aluminum 6061 subjected to thermal cycling treatment using electrochemical impedance spectroscopy (EIS), Corros. Sci. 51 (2009) 2493–2501.

[25] H. Fang, S. Nesic, B. Brown, S. Wang, General CO_2 Corrosion in High Salinity Brines, CORROSION/2006, Paper No. 6372, NACE, Houston, TX, 2006.

[26] S. Nesic, S. Wang, H. Fang, W. Sun, J.K.-L. Lee, A New Updated Model of CO_2/H_2S Corrosion in Multiphase Flow, CORROSION/2008, Paper No. 8535, NACE, Houston, TX, 2008.

[27] M. Shayegani, A. Afshar, M. Ghorbani, M. Rahmaniyan, Mild steel carbon dioxide corrosion modeling in aqueous solutions, Corros. Eng. Sci. Technol. 43 (4) (2008) 290.

[28] S. Nesic, J. Postlethwaite, S. Olsen, An Electrochemical Model for Prediction of CO_2 Corrosion, CORROSION/95, Paper No. 131, NACE, Houston, TX, 1995.

[29] J. Han, Y. Yang, B. Brown, S. Nesic, Electrochemical Investigation of Localized CO_2 Corrosion on Mild Steel, CORROSION/2007, Paper No. 7323, NACE, Houston, TX, 2007.

[30] O.A. Nafday, S. Nesic, Iron Carbonate Scale Formation and CO_2 Corrosion in the Presence of Acetic Acid, CORROSION/2005, Paper No. 5295, NACE, Houston, TX, 2005.

[31] W. Sun, S. Nesic, Kinetics of corrosion layer formation: Part 1 – iron carbonate layers in carbon dioxide corrosion, Corrosion 64 (2008) 4.

[32] W. Sun, S. Nesic, S. Papavinasam, Kinetics of iron sulfide and mixed iron sulfide/carbonate scale precipitation in CO_2/H_2S corrosion, CORROSION/2006, Paper No. 6644, NACE, Houston, TX, 2006.

[33] D.A. Lopez, W.H. Schreiner, S.R. de Sanchez, S.N. Simison, The influence of carbon steel microstructure on corrosion layers an XPS and SEM characterization, Appl. Surf. Sci. 2007 (2003) 69–85.

[34] A. Dugstad, L. Lunde, K. Videm, Parametric Study of CO_2 Corrosion of Carbon Steel, CORROSION/94, Paper No. 14, NACE, Houston, TX, 1994.

[35] E.W.J. van Hunnik, B.F.M. Pots, E.L.J.A. Hendriksen, The Formation of Protective FeCO3 Corrosion Product Layers in CO_2 Corrosion, CORROSION/96, Paper No. 6, NACE, Houston, TX, 1996.

[36] G.A. Zhang, Y.F. Cheng, Corrosion of X65 steel in CO_2 – saturated oilfield water in the absence and presence of acetic acid, Corros. Sci. 51 (2009) 1589–1595.

[37] G.A. Zhang, Y.F. Cheng, On the fundamentals of electrochemical corrosion of X65 steel in CO_2-containing formation water in the presence of acetic acid in petroleum production, Corros. Sci. 51 (2009) 87.

[38] P. Li, T.C. Tan, J.Y. Lee, Impedance spectra of the anodic dissolution of mild steel in sulfuric acid, Corros. Sci. 38 (1996) 1935.

[39] G. Zhang, C. Chen, M. Lu, C. Chai, Y. Wu, Evaluation of inhibition efficiency of an imidazoline derivative in CO_2 – containing aqueous solution, Mater. Chem. Phys. 105 (2007) 331–340.

[40] J. Baptiste, M.E. Orazem, N. Pébère, B. Tribollet, CPE analysis by local electrochemical impedance, Electrochim. Acta 51 (2006) 1473–1479.

[41] O. Devos, C. Gabrielli, B. Tribollet, Simultaneous EIS and in situ microscope observation on a partially blocked electrode application to scale electrodeposition, Electrochim. Acta 51 (2006) 1413–1422.

[42] E. Remita, B. Tribollet, E. Sutter, V. Vivier, F. Ropital, J. Kittel, Hydrogen evolution in aqueous solutions containing dissolved CO_2: quantitative contribution of the buffering effect, Corros. Sci. 50 (2008) 1433.

[43] M.E. Orazem, N. Pebere, B. Tribollet, Enhanced graphical representation of electrochemical impedance data, J. Electrochem. Soc. 153 (4) (2006) B129–B136.

[44] A. Dugstad, Fundamental Aspects of CO_2 Metal Loss Corrosion, Part I: Mechanism, CORROSION/2006, Paper No. 6111, NACE, Houston, TX, 2006.

[45] M. Ueda, H. Takabe, Effect of Environmental Factor and Microstructure on Morphology of Corrosion Products in CO_2 Environments, CORROSION/99, Paper No. 13, NACE, Houston, TX, 1999.

[46] A. Dugstad, H. Hemmer, M. Seiersten, Effect of Steel Microstructure upon Corrosion Rate and Protective Iron Carbonate Film Formation, CORROSION/2000, Paper No. 24, NACE, Houston, TX, 2000.

[47] M.B. Kermani, A. Morshed, Carbon dioxide corrosion in oil and gas production – a compendium, Corrosion 59 (2003) 8.